Segmentation of myocardial boundaries in tagged cardiac MRI using active contours: a gradient-based approach integrating texture analysis

A. Histace[1], B. Matuszewski[2], Yan Zhang[2]

[1]ETIS UMR CNRS 8051, F-95000 Cergy, France
[2]ADSIP, University of Central Lancashire, United Kingdom
Corresponding author: aymeric.histace@ensea.fr

Abstract. The non invasive assessment of cardiac function is of first importance for the diagnosis of cardiovascular diseases. Among all medical scanners only a few enables radiologists to evaluate the local cardiac motion: Tagged Cardiac MRI is one of them. This protocol generates on Short-Axis (SA) sequences a dark grid which is deformed in accordance with the cardiac motion. Tracking the grid allows specialists a local estimation of cardiac geometrical parameters within myocardium. The work described in this paper aims to automate the myocardial contours detection in order to optimize the detection and the tracking of the grid of tags within myocardium. The method we have developed for endocardial and epicardial contours detection is based on the use of texture analysis and active contours models. Texture analysis allows us to define energy maps more efficient than those usually used in active contours methods where attractor is often based on gradient and which were useless in our case of study, for quality of tagged cardiac MRI is very poor.

1 Introduction

Non invasive assessment of the cardiac function is of major interest for the diagnosis and the treatment of cardiovascular pathologies. Whereas classical cardiac MRI only enables radiologists to measure anatomical and functional parameters of the myocardium (mass, volume...), tagged cardiac MRI makes it possible to evaluate local intramyocardial displacements. For instance, this type of information can lead to a precise characterization of the myocardium viability after an infarction. Moreover, data concerning myocardium viability makes it possible to decide of the therapeutic : medical treatment, angiopathy, or coronary surgery and following of the amelioration of the ventricular function after reperfusion.

The SPAMM (Space Modulation of Magnetization) acquisition protocol [1] we used for the tagging of MRI data, displays a deformable 45-degrees oriented dark grid which describes the contraction of myocardium (Fig. 1) on the images of temporal Short-Axis (SA) sequences. Thus, the temporal tracking of the

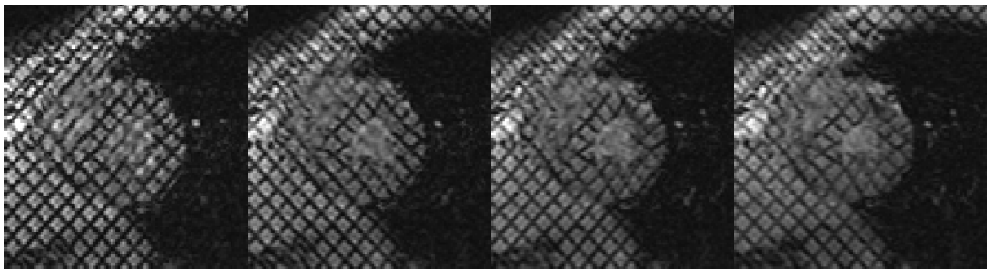

Fig. 1. Short-Axis-Tagged MRI acquisition between end-diastole and end-systole.

grid can enable radiologists to quantify cardiac geometrical parameters within myocardium.

Numerous studies were carried out concerning the analysis of the deformations of the grid of tags on SA sequences[1]: First part of them are based on a direct estimation of the displacement field of the myocardium [4–13], the other part on an indirect estimation of the displacement field [14–25].

A common step of all these approaches is the segmentation of myocardial boundaries for each instant of Left Ventricular (LV) contraction (diastole)[2] (see Fig. 2 for a manual segmentation of these boundaries).

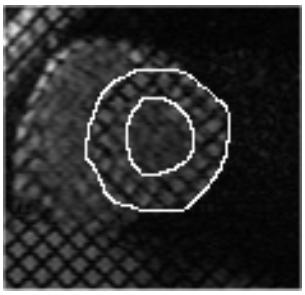

Fig. 2. Manual detection of epicardial (external circle) and endocardial (internal circle) boundaries of the Left Ventricle (LV) on a Short-Axis-Tagged MRI acquisition.

This segmentation step is of primary importance since detection and tracking of the grids are made on this particular area for locally quantified LV displacements.

[1] Following cited articles are, for a majority of them, former ones. For a complete study author by author see [2, 3].

[2] Left Ventricle contraction represents 80% of the whole heart contraction function.

Among all previous cited papers, the only study integrating automatic detection of endocardial and epicardial boundaries within the tracking of the grid process was developed by Guttman [26] and carried out on radially-tagged acquisitions (Fig. 3).

Fig. 3. Radially tagged cardiac MRI taken from [26].

This method based on a prior erasure of tags using non linear filtering, turned out to be inappropriate to our images which are not radially tagged as one can notice on Fig. 1. Moreover, this particular type of tagging is no more used in medical literature.

All other works dealing with this detection problem involve manual detection of the myocardial boundaries [27, 28, 16], or a detection previously made on classical cardiac MRI sequences [2] or on filtered ones [3] and then do not entirely answer to the problem of in routine application.

As a consequence, we present, in this article, an alternative method for the automatic detection of myocardial boundaries on tagged cardiac MRI which integrates active contours and texture analysis. Our method enables an automatic detection of myocardial boundaries of LV on SA sequences and then an optimized tracking of the grid of tags within myocardium is possible.

Concerning the layout of this paper, next section is dedicated to the presentation of the global segmentation method of myocardial boundaries. Section 3 and 4 deals with the computation of what we call energy maps thanks texture analysis. Following section presents visual results of segmentation obtained on different patients and a statistical validation of the developed method. Last section is dedicated to discussion.

2 Active contours and context

Originally proposed in [29], active contours for segmentation have attracted extensive research in the past two decades. The basic idea of the active contour is to iteratively evolve an initial curve towards the boundaries of the target objects driven by the combination of internal forces determined by the geometry of the evolving curve and the external forces induced from the image.

Image segmentation methods using active contours are usually based on minimising functionals which are so defined that curves close to the target boundaries have small values. For instance, in [29], authors formerly proposed the following functional:

$$E(C) = \alpha \int_0^1 |C'(q)|^2 dq + \beta \int_0^1 |C''(q)|^2 dq - \lambda \int_0^1 |\nabla u_0(C(q))| dq \quad (1)$$

where $C(q)$ is a parameterized flat curve, u_0 the initial image data and α, β, λ are positive constant. The first two parameters α, β control the regularity of the curve (E_{intern}) and λ controls the attraction of the curve to the targeted boundaries (∇u_0, with ∇ the classical gradient operator) of the studied image u_0 (E_{extern}). To solve these functional minimisation problems, a corresponding partial differential equation is constructed as the Gateaux derivative gradient flow resulting in a curve evolution.

Practically speaking, to obtain interesting results with minimisation of Eq. (1), initialization of the curve has to be made close to the boundary to segment. This drawback is directly linked to the computation of the external energy induced from the image which is based on a classical gradient operator: As a consequence, if the initialization of the curve is made too far from the targeted structure, other local minima of the image gradients can corrupt final segmentation result.

However, in the global scheme of medical image segmentation, in order not to be too time consuming, initialization of the curve has to be easy and fast and then not necessarily close from the target. For instance, initialization is often made from the borders of the studied image, or from the gravity center of a particular Region of Interest.

Taking this into consideration, we propose an evolution of the functional described by Eq. (1) given by:

$$E(C) = \alpha \int_0^1 |C'(q)|^2 dq + \beta \int_0^1 |C''(q)|^2 dq - \lambda \int_0^1 |\nabla u_{map}(C(q))| dq + \kappa \int_0^1 \boldsymbol{n}(C(q)) dq \quad (2)$$

As one can notice, two terms are added to the classical functional. The last one, $\kappa \int_0^1 \boldsymbol{n}(C(q))dq$ is a classical balloon energy formerly introduced in [30]. To explain its interest, let's consider a circle as the initializing curve which evolution law is only driven by this energy with $\kappa > 0$. For each step of the evolution process, the circle has no other solution than to spread all along its local normals ($\boldsymbol{n}$): The diameter of the circle grows up. It is an extra expanding term usually found necessary for quicker convergence. This energy has shown to

be useful for fast growing of the curve when initialization is made far from the targeted boundary.

The term given by $\lambda \int_0^1 |\nabla u_{map}(C(q))| dq$ is derived from the former one of Eq. (1) and represents the induced boundary energy (E_{extern}) adapted to our particular domain of application: Tagged cardiac MRI. Indeed, the grid of tags does not allow us to obtain a good gradient attractor for myocardial contours, for the gradient underscored the grid of tags (Fig. 4) and not the myocardial boundaries (see Fig. 2). As a consequence, the boundary-based energy is computed from a preprocessed version u_{map} of original image u_0 which is described next section.

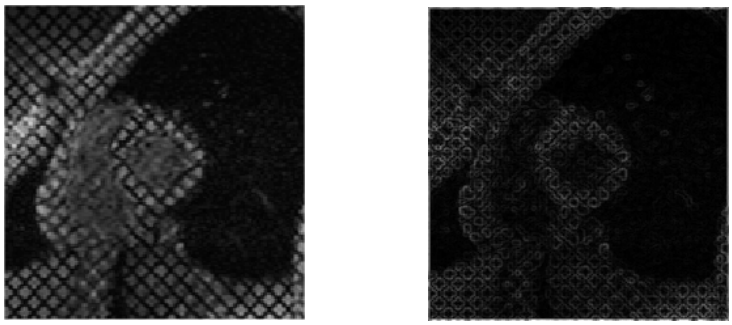

(a) (b)

Fig. 4. (a) Original Image, (b) Norm of the corresponding gradient. As one can notice, the grid of tags does not allow us to obtain a good gradient attractor for myocardial contours.

We shall now describe how to obtain u_{map} images for both endocardial and epicardial boundaries.

3 Computations of u_{map} images

3.1 Endocardial boundary

A major property observed on SA tagged MRI sequences is the fast erasure of tags in the cardiac cavity due to blood circulation (see Fig. 1). To explain this phenomenon, one must understand that tagging process is obtained thanks a saturation of hydrogen kernels in surfaces orthogonal to main orientations of the grid (see [1] for complete description of the process). As a consequence, muscles, fat tissues and blood are tagged. But, considering cardiac motion, between two phases of contraction, blood is pumped out of the cardiac cavity into the main circulation. Therefore, tagged cells of blood are no more visible during acquisition process as soon as contraction has begun.

This property is of primary importance since image can be roughly divided into two areas : a tagged area (1) where the tracked grid remains visible and an homogenous area (2) , roughly the cardiac cavity of Left and Right ventricles, where tagged are no more visible. As a consequence, area (1) and (2) can be easily discriminated by simple texture parameters calculated on a local kernel like mean, and standard deviation: Area (1) is characterized by a standard deviation more important than area (2) which is more homogenous (absence of tagging). For both areas, characterizing means remain nearly the same.

Considering this, we propose the calculation of a mean (M)-standard deviation (σ) image to build a precise gradient-based energy to detect the endocardial boundary (Fig. 5c). This map is obtained by computation of Eq. (3) on the processed original sampled image $u_0(i,j)$ where (i,j) denotes the indices of a given pixel:

$$u_{map}^{endo}(i,j) = w_m.m_N(i,j) - w_\sigma.\sigma_N(i,j) \qquad . \tag{3}$$

w_m and w_σ are respectively the weights given to the mean computed on a kernel of size $N * N$ centered on the processed pixel and the weight given to the standard deviation computed with the same kernel. w_m and w_σ verify $w_m + w_\sigma = 1$.

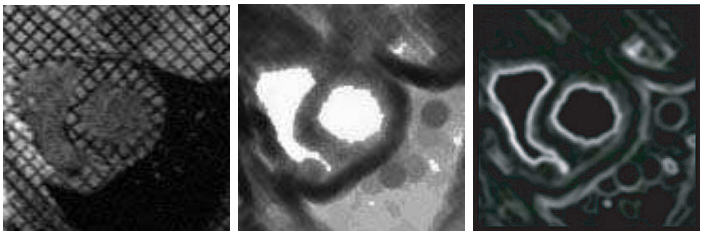

(a) (b) (c)

Fig. 5. (a) Original Image u_0, (b) Computation of u_{map}^{endo} $(\frac{w_\sigma}{w_m}) = 2$ and $N = 11$, (c) ∇u_{map}^{endo}.

As one can notice on Fig. 5.b, the computation of the mean-standard deviation image makes enhancement of the cardiac cavities of LV possible (pixels of high intensity). This image leads, on the one hand, to a possible automatic detection of the center of the LV cardiac cavity (that can be used for active contour initialization), and, on the other hand, to a gradient-based energy (Fig. 5.c) totally adapted to our purpose.

3.2 Epicardial boundary

The gradient based energy for the segmentation of the epicardial contour was more complex to compute since, as one can see on Fig. 1, the boundary is hard

to detect visually even for experts. Moreover, as for endocardial contour, active-contour segmentation can not simply integrate tagged MRI gradient as attractor, for induced gradient-based energy is not adapted as shown before.

As a consequence, to compute a useful u_{map}^{epi}, it appeared interesting to analyze the particular texture of the lung (dark area situated on the right of Fig. 1). This area, compared with the rest of tagged MRI, is described by a rough texture. Thus, the use of second order texture parameters and more particularly, the calculation of the co-occurrence matrix entropy on a $N * N$ block, can make the enhancement of the lung area possible by characterizing it with high entropy coefficients (Fig. 6.b). The map u_{map}^{epi} then obtained allows us to compute an interesting gradient-based energy (Fig. 6.c).

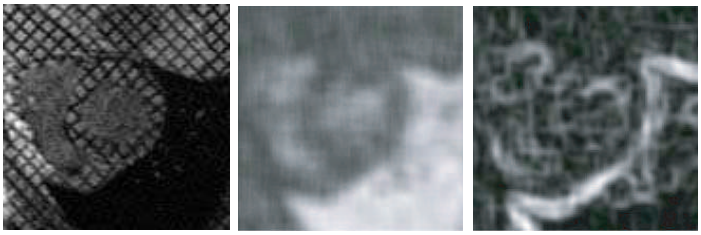

(a) (b) (c)

Fig. 6. (a) Original Image, (b) Computation of u_{map}^{epi} $(N = 5)$, (c) ∇u_{map}^{epi}.

4 Practical implementation

4.1 Computation

Practically speaking, in order to perform a quick computation, detection (on the first image of the sequence) and tracking of the myocardial boundaries (on the other images describing diastole) are made separately : the detection method is divided into five steps :

1. u_{map}^{endo} is first computed and barycenter of the LV cavity is used for automatic active contour initialization (a circle) (Figs. 7.a and 7.b),

2. considering the given automatic initialization of step 1, a first fast growing (only taking into account the balloon force) of the active contour is used to obtain a rough segmentation of the endocardial contour,

3. the resulting curve from step 2 is then used as initialization for boundary-based evolution considering corresponding term of Eq. (2) with $u_{map} = u_{map}^{endo}$ (Fig. 7.b),

4. since epicardial contour is situated close to the endocardial one (see Fig. 2), an automatic radial spreading of the curve detected step 3 (no more than 4 pixels) is performed to obtain a rough segmentation of it,

5. the curve of step 4 is then used as initialization for boundary-based evolution considering corresponding term of Eq. (2) with $u_{map} = u_{map}^{epi}$ (Fig. 7.c).

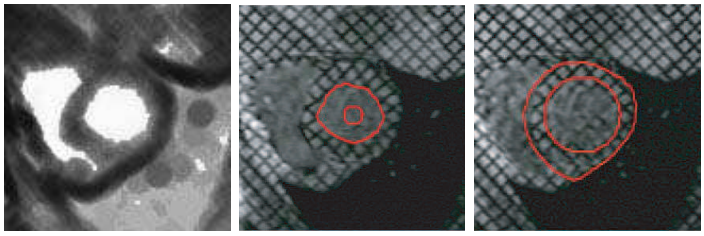

(a) (b) (c)

Fig. 7. (a) Computation of u_{map}^{endo} ($\frac{w_\sigma}{w_m}$) = 2 and $N = 11$ for automatic localization of the barycenter of LV cavity, (b) initialization and detection of endocardial boundary, (c) initialization and detection of epicardial boundary.

Considering now tracking, in order to have a quick implementation, each detected myocardial boundaries (endocardial and epicardial) at instant t of the diastole is used as initialization for a boundary-based evolution at instant $t+1$.

For epicardial contour detection and tracking, concerning part of the contour where gradient-based energy fails to bring good attraction (left part of the boundary), the coherence of the detection is obtained by setting to zero the λ parameter of Eq. (2). To do so, a test of distance (Euler) between the new calculated coordinates of the active contour point and the center of the LV cavity is computed. Indeed, compared to endocardial contour, global displacement of the epicardial one still less important. As a consequence, if distance to the center of the new coordinates control point appears to be incoherent (to far from the precedent one), calculation is made again with $\lambda = 0$: Geometrical constrains are privileged to ensure coherence of the result.

4.2 Results

Fig. 8 shows results of detection for 5 different patients (extracted from a global set of 8).

Considering first intrinsic performances of the proposed method, as one can notice, the implemented method is robust as regard of the initialization which is always the same in each different case. Moreover the developed method is reproducible and does not need new tuning of the different parameters for new

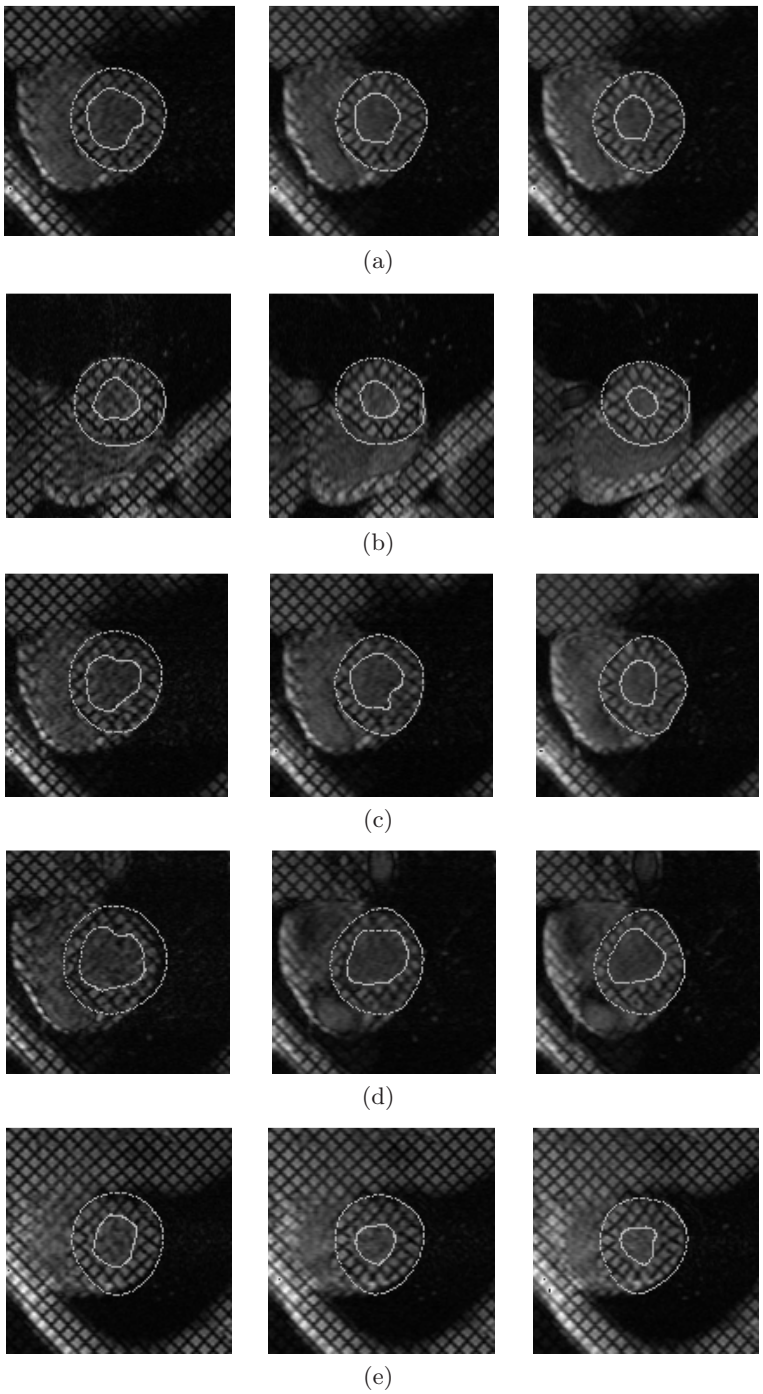

Fig. 8. Detection and tracking of endocardial and epicardial boundaries on SA sequences all along diastole for 5 different patients.

patients as shows Fig. 8 where all segmentation have been made with same setting of the different parameters presented in previous section.

Considering now performances of the proposed approach in terms of precision, we propose a first statistical analysis made on a set of 8 patients as a basis for a future more complete analysis made on a larger scale. More precisely, for each of the 8 patients, 6 images extracted from a synchronized systole acquisition made at a median slice level of the LV are considered. For each image of a particular sequence, the semi-automatic segmentation of endocardial and epicardial boundaries of the LV and the corresponding myocardial surface is generated (see Fig. 9.a). The same study, starting from a manual expert segmentation of the myocardial boundaries, is also performed (see Fig. 9.b). For each image of a sequence, automatic and manual surfaces are compared (see Fig. 9.c) thanks to a calculation of the ratio corresponding to the matching and non-matching pixels.

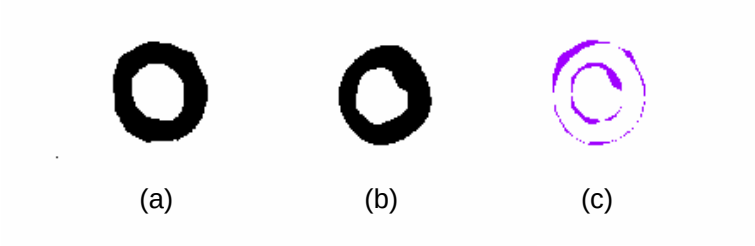

Fig. 9. Detection mask obtained after segmentation of myocardial boundaries on a particular image: (a) expert's mask (manual segmentation), (b) automatically segmented mask (presented method), (c) superposition of both (dark surface stands for mismatched pixels of both segmentation).

More precisely, each pixel of the automatic generated mask is identified as being a True Positive (TP) pixel or a False Positive (FP) pixel or a True Negative (TN) pixel or at last a False Negative (FN) pixel. Tab. 1 shows the average number of each type of pixels (expressed in percentage of the average total number of pixels of each pixel class within manual generated myocardium surface) for each of the 6 considered time steps of the systole.

Calculation of the ratio between matching pixels of both surfaces (TP) shows that for 48 processed images (6 per patients) more than 80% of the different surfaces are matching. Moreover, only more or less 3% of the automatic detected pixels are considered as FP, that is to say that they do not match at all expert surface. Those pixels are often situated near endocardial boundaries. This is above all due to the papillaries muscles of the LV which are also tagged and as a consequence influence expert segmentation (they tend to integrate them within the cardiac cavity). One can notice that in this case, the expert's segmentation of endocardial boundaries can lead to an overestimation of the surface area of

Systole Step	**Step 1**	**Step 2**	**Step 3**	**Step 4**	**Step 5**	**Step 6**
TP	87.2%	85.1%	81.4%	79.7%	82.1%	81.0%
FP	3.1%	2.9%	2.2%	2.1%	1.9%	2.1%
TN	92.1%	93.1%	89.3%	90.1%	94.3%	91.8%
FN	1.2%	1.6%	1.9%	2.3%	1.7%	2.1%

Table 1. Average number of each type of pixels (expressed in percentage of the average total number of pixels of each pixel class within manual generated myocardium surface) for each of the 6 considered time steps of the systole.

LV's cavity since papillaries muscle must not be taken into account (which is the case with proposed automatic method).

No comparison with others method are proposed since, as we mentioned it before, proposed automatic methods of the literature are not directly performed on tagged cardiac MRI but always on classical cardiac MRI (double acquisition).

5 Conclusion and outlooks

In this article, we propose an automatic approach for segmentation of epicardial and endocardial boundaries of the LV directly on tagged cardiac MRI. The detection of the endocardial and epicardial boundaries on SA sequences is fully automatic and satisfactory, whereas the literature always involves manual detection during the analysis of tagged MR images. About the results of the detection of the epicardial contours, the method allows us to obtain satisfying results which are in agreement with medical specialists opinion. The method is less robust than for endocardial segmentation, but still good, and the way we initialize the segmentation allows us not to be too dependant of this important step. The fact that even visually, detection still very difficult for radiologists is particularly important for the consideration of our results.

As far as the robustness is concerned, progresses still to be done in the way the segmentation is function of the variation of the weights of the different energies which are computed and the size N of the neighborhood on which are computed the texture map.

Regarding precision of the method, we have presented a first statistical study which shows very promising results. If this statistical study still to be strengthened in order to characterize intra and inter operator variabilities, obtained estimation allows us to go to a further step in the use of the proposed method: it is now possible to use these results (shared with those given by the tracking of the grids on SA) to develop a $2D + T$ analysis of the myocardium. The aim of this study will be the calculation of local cardiac quantitative parameters correlated to "gold standards ones" (like fraction ejection) in order to early reveal eventual pathologies like ischemia for example but also to characterize myocardial viability after reperfusion.

First results have been already obtained. Classical cardiac parameters on 10 SA sequences as radial, circumferential, longitudinal displacements, torsion or

deformations have been calculated. We present in Tab.2 a comparison between our obtained results for the quantification of the radial displacements and two studied of the medical literature.

	Base	Median	Apex
[31] (12 patients)	5.9 ± 0.4	6 ± 0.3	4.65 ± 0.2
[32] (31 patients)	5.0 ± 1.3	4.3 ± 1.1	4.2 ± 1.6
Our estimation (10 patients)	5.7 ± 0.5	4.9 ± 0.7	4.3 ± 0.9

Table 2. Comparison between our quantification and two studies of the medical literature concerning the estimation of the radial displacements (expressed in millimeters) for healthy volunteers.

As one can notice, our results are comparable to those of the medical literature.

Moreover, it is also possible to realize a two-dimensional temporal map (according to the recommendations of the American Heart Association) characterizing the local displacements and local deformations of the myocardium (Figure 10).

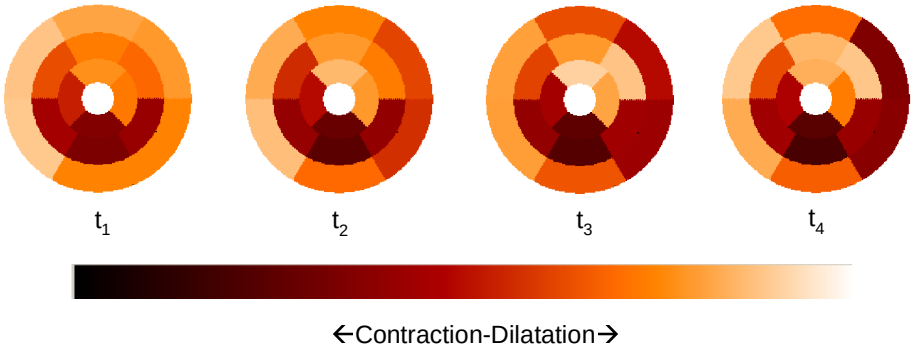

Fig. 10. Radial contraction of the heart represented in accordance with the AHA's recommendations.

Presented results could be interesting for radiologists to evaluate torsion, shearing, longitudinal and radial displacements of the LV and then to draw early diagnoses of particular cardiopathies. These first results needs now to be confirmed through a more complete clinical validation.

6 Acknowledgement

This work has been financially supported by ECSON project (EPSRC grant No. EP/F013698/1, www.ecson.org).

References

1. Zerhouni, E., Parish, D., Rogers, W., Yang, A., Shapiro, E.: Human heart : tagging with MR imaging - a method for noninvasive assessment of myocardial motion. Radiology **169** (1988) 59–63
2. Petitjean, C., Rougon, N., Cluzel, P.: Assessment of myocardial function: A review of quantification methods and results using tagged MRI. Journal of Cardiovascular Magnetic Resonance **7** (2005) 501–516
3. Axel, L., Chung, S., Chen, T.: Tagged mri analysis using gabor filters. In: Biomedical Imaging: From Nano to Macro, 2007. ISBI 2007. 4th IEEE International Symposium on. (2007) 684–687
4. Prince, J., McVeigh, E.: Motion estimation from tagged MR image sequences. IEEE Transactions on Medical Imaging **11** (1992) 238–249
5. Gupta, S., Prince, J.: On variable brightness optical flow for tagged MRI. In Kluwer, ed.: Information Processing in Medical Imaging, Dordrecht (Pays-Bas), Kluwer (1995) 323–334
6. Gupta, S., Prince, J., Androutsellis-Theotokis, S.: Bandpass optical flow for tagged MRI. In: International Conference on Image Processing. Volume 3., San Diego CA (1997) 364–367
7. Dougherty, L., Asmuth, J., Blom, A., Axel, L., Kumar, R.: Validation of an optical flow method for tag displacement estimation. IEEE Transactions on Medical Imaging **18** (1999) 359–363
8. Osman, N., Mc Veigh, E., Prince, J.: Imaging heart motion using Harmonic Phased MRI (HARP). IEEE Transactions on Medical Imaging **19** (2000) 186–202
9. Haber, I., Kikinis, R., Westin, C.: Phase-driven finite elements model for spatio-temporal tracking in tagged mri. In: Proceedings of Fourth International Conference On Medical Image Computing and Computer Assisted Intervention (MICCAI'01). (2001) 1352–1353
10. Chandrashekara, R., Mohiaddin, R., Rueckert, D.: Analysis of myocardial motion in tagged MR images using nonrigid image registration. In: Medical Image Understanding and Analysis, Porthmouth (2002)
11. Petitjean, C., Rougon, N., Prêteux, F., Cluzel, P., Grenier, P.: A non rigid registration approach for measuring myocardial contraction in tagged mri using exclusive f-information. In: Proceedings International Conference on Image and Signal Processing (ICISP'2003), Agadir, Morocco. (2003)
12. Rougon, N., Petitjean, C., Prteux, F., cluzek, P., Grenier, P.: A non-rigid registration approach for quantifying myocardial contraction in tagged MRI using generalized information measures. Medical Image Analysis **9** (2005) 353–375
13. Oubel, E., De Craene, M., Gazzola, M., Hero, A., Frangi, A.: Multiview registration of cardiac tagging mri images. In: Biomedical Imaging: From Nano to Macro, 2007. ISBI 2007. 4th IEEE International Symposium on. (2007) 388–391
14. Kumar, S., Goldgof, D.: Automatic tracking of SPAMM grid and the estimation of deformation parameters from cardiac MR images. IEEE Transactions on Medical Imaging **13** (1994) 122–132

15. Kraitchman, D., Young, A., Chang, C., Axel, L.: Semi-automatic tracking of myocardial motion in MR tagged images. IEEE Transactions on Medical Imaging **14** (1995) 422–433
16. Young, A., Kraitchmann, D., Dougherty, L., Axel, L.: Tracking an finite element analysis of stripe deformation in magnetic resonance tagging. IEEE Transactions on Medical Imaging **14** (1995) 413–421
17. Radeva, P., Amini, A., Huang, J.: Deformable B-solids and implicit snakes for 3D localization and tracking of SPAMM MRI data. Computer Vision and Image Understanding **66** (1997) 163–178
18. Amini, A., Chen, Y., Curwen, R., Mani, V., Sun, J.: Coupled B-snake grids and constrained thin-plate splines for analysis of 2D tissue deformations from tagged MRI. IEEE Transaction on Medical Imaging **17** (1998) 344–356
19. Urayama, S., Matsuda, T., Sugimoto, N., Mizuta, S., Yamada, N., Uyama, C.: Detailed motion analysis of the left ventricular myocardium using an MR tagging method with a dense grid. Magnetic Resonance in Medicine **44** (2000)
20. Clarysse, P., Bracoud, L., Croisille, P., Magnin, I.: Integrated quantitative analysis of tagged magnetic resonance images. FIMH-LNCS **2230** (2001) 69–75
21. Histace, A., Cavaro-Ménard, C., Courboulay, V., Ménard, M.: Analysis of tagged cardiac mri sequences. Lecture Notes on Computer Science (Proceedings of the 3rd Functional Imaging and Modelling of the Heart (FIMH) Workshop) **3504** (2005) 404–413
22. Zhang, S., Douglas, M., Yaroslavsky, L., Summers, R., Dilsizian, V., Fananapazir, L., Bacharach, S.: A fourier based algorithm for tracking SPAMM tags in gated magnetic resonance cardiac images. Medical Physics **32** (1996) 1359–1369
23. Groot-Koerkamp, M., Snoep, G., Muijtjens, A., Kemerink, G.: Improving contrast and tracking of tags in cardiac magnetic resonance images. Magnetic Resonance in Medicine **41** (1999) 973–982
24. Guttman, M., Zerhouni, E., McVeigh, E.: Analysis of cardiac function from MR images. IEEE Computer Graphics and Applications **17** (1997) 30–38
25. Denney, T.: Estimation and detection of myocardial tags in MR images without user-defined myocardial contours. IEEE Transactions on Medical Imaging **18** (1999) 330–344
26. Guttman, M., Prince, J., McVeigh, E.: Tag and contour detection in tagged MR images of the left ventricle. IEEE Transactions on Medical Imaging **13** (1994) 74–88
27. Amini, A., Chen, Y., Elayyadi, M., Radeva, P.: Tag surface reconstruction and tracking of myocardial beads form SPAMM-MRI with parametric B-Spline surfaces. IEEE Transactions on Medical Imaging **20** (2001) 94–103
28. Haber, I., Metaxas, D., Axel, L.: Three-Dimensional motion reconstruction and analysis of the right ventricle using tagged MRI. Medical Image Analysis (2000) 335–355
29. Kass, M., Witkin, A., Terzopoulos, D.: Snakes: Active contour models. International Journal of Computer Vision **1** (1988) 321–331
30. Cohen, L., Cohen, I.: Finite element methods for active contour models and balloons for 2d and 3d images. IEEE Transactions on Pattern Analysis and Machine Intelligence **15** (1993) 1131–1147
31. Young, A., Kramer, C., Ferrari, V., Axel, L., Reichek, N.: Three-dimensional left ventricular deformation in hypertrophic cardiomyopathy. Circulation **90** (1994)
32. Moore, C., Lugo-Olivieri, C., McVeigh, E., Zerhouni, E.: Three dimensional systolic strain patterns in the normal human left ventricle: Characterization with tagged mr imaging. Radiology **214** (2000) 453–466